

Effect of Chloride Ions on Corrosion Behavior of High Tensile Strength Steel Rebar in the Synthetic Concrete Pore Solution Prepared with Tap Water

Ahmed Kareem Abdulameer* and Saheb Mohammed Mahdi

Materials Engineering Department, College of Engineering, Mustansiriyah University, Baghdad, Iraq.

Received 27 July 2022; Accepted 22 December 2022

Abstract

In this work, the electrochemical corrosion behavior of carbon steel grade 80 (with a minimum yield strength of 550 MPa) was studied in a simulated concrete pore solution containing chloride ions at different concentrations. The solution was prepared with tap water and contaminated with chloride at concentrations of (0, 0.5, 1, 1.5, and 2% as weight percent). Three electrode system was used in the electrochemical measurements. All the measurements were done at room temperature of (25 ± 1 °C). Open circuit potential, Tafel extrapolation plot, and cyclic potentiodynamic polarization were utilized in this study. The surface morphologies were investigated by using an optical microscope and Scanning Electron Microscope supplied with Energy Dispersive X-Ray (EDX) Analysis. The results showed that the corrosion potential shifted in a noble direction (from -400mV to -350mV) and the corrosion rate of the steel samples increased (from 0.347µm/y to 0.519µm/y) with the addition of 1% NaCl. Then the potential shifted in an active direction of (-392mV) and the corrosion rate was decreased by (12.3%) with the addition of 2% NaCl, due to the reduction of dissolved oxygen with increased chloride concentration, and the effect of the barrier layer that formed. In addition, the cyclic polarization showed metastable pitting corrosion on the steel surface at the addition of 1% NaCl, and loss of the passivation layer at 1.5% NaCl with the formation of stable pitting corrosion. The critical chloride level was 0.5% NaCl addition. The EDX indicates that corrosion occurs at MnS inclusions sites.

Keywords: Reinforcement corrosion, synthetic concrete pore solution, tap water, potentiodynamic cyclic polarization, Tafel plot.

1. Introduction

To preserve the same mechanical qualities throughout the lifespan of a concrete structure, steel reinforcement must be durable and corrosion-resistant [1, 2]. Some reinforced concrete structures, such as ocean structures and bridges, are subjected to severe aggressive conditions, in addition to the applied stresses [3]. However, the construction may be destroyed by corrosion of carbon steel if the passive layer of the steel surface is fractured [4]. Concrete's alkaline pore solutions protect the steel in the concrete from corrosion. In certain cases, the protective coating might be penetrated, leading the rebar to corrode. The most frequent ion that may damage passivated steel is chloride [5]. The process of corrosion by chloride ions, especially in the coastal environment, is one of the most crucial challenges [4, 6, 7].

In many aspects, pitting and crevice attacks are quite identical. Both pitting and crevice rusting possess specified threshold potential, and the effects of micro-alloying or additive elements as well as the environmental conditions on resistance to corrosion are the same [8, 9]. When it comes to the initiation process in these two cases there are a few notable variations, such as the location of the start and the pH change. As a result of the hydrolysis process between metal ions in the crevice corrosion and the formation of hydrogen ions, pH lowers continually until it reaches virtually zero [9, 10] in crevice corrosion. De-passivation pH occurs at this stage, and the passive coating breaks down, allowing crevice corrosion to start. Pitting is a kind of localized corrosion

where the attack is concentrated on a specific region of the surface of a metal. When a passive film starts to break down in a specific area, it causes pitting. This kind of corrosion has two stages: initiation and propagation, similar to crevice corrosion. The breaking of the passive layer and the development of the anodic current at the surface of the metal will both be included in the definition of the initiation stage. [11, 12].

Many investigations have concluded that chloride-induced corrosion onset has been under anodic control, which implies that corrosion is limited by steel electrochemical characteristics such as anodic Tafel coefficients, anodic potential, and current [13-15]. In practice, corrosion is believed to begin when the chloride concentration at the surface of the reinforcing bars exceeds a critical threshold level termed (C_{crit}). Numerous explanations of "corrosion initiation" prevail, resulting in diverse C_{crit} estimations. Some researchers identify the onset of corrosion only with the de-passivation of reinforcing steel, which is closer to the transfer from the initiation stage to the propagation stage. Whereas others identify that with an acceptable level of corrosion and it's a part of the corrosion propagation stage. A theoretical and practical point of view suggests that corrosion initiation is not an immediately happening, but rather a gradual phase before corrosion stabilizes. As a result, C_{crit} levels documented in the previous research are scattered over two orders of magnitude. Many service life design codes for concrete buildings utilize C_{crit} values that are really different [16, 17]. Chloride ion concentration levels for corrosion prevention are listed in Tab.1 based on various codes and regulations, including

*E-mail address: ebma042@uomustansiriyah.edu.iq

ISSN: 1791-2377 © 2023 School of Science, IHU. All rights reserved.

doi:10.25103/jestr.161.16

cementitious materials, aggregates, mixing water, and as well as admixtures [18].

MAHIMA et al. [19] collected chloride threshold values from extensive investigations that have been published in the recent two decades. They showed that, depending on

exposure circumstances and the local surroundings, the literature indicates a significant differences in C_{crit} level for the same kind of steel. Also, they identified several factors that affected the C_{crit} level, as shown in Fig. 1.

Table 1. Maximum chloride content in concrete for different codes and standards [18].

Code / standard	Type or use of concrete	Cl ⁻ % by wt. of cement (maximum limits)		
		Water-soluble chloride		Acid-soluble chloride
201.2R-92	- RC	0.10 – 0.15		
	- Prestressed concrete	0.06		
	- Dry, above-ground concrete	no limit		
ACI 318 – 2002 & Code of the Philippines	- RC exposed to chloride in service	0.15		
	- RC that will be dry or protected from moisture in service	1.00		
	- Prestressed concrete	0.06		
	- Other reinforced concrete construction	0.30		
ACI 222 - 1997	- RC in wet conditions	ASTM C1218	Soxhlet	ASTM C1152
	- RC in dry conditions	0.08	0.08	0.1
	- RC in dry conditions	0.15	0.15	0.2
	- Prestressed concrete	0.06	0.06	0.08
BS EN206-1 BS/8500 ¹	- RC made with cement conforming to BS 4027	0.20		
	- RC or concrete containing embedded metal made with other cement types	0.40		
	- Concrete without reinforcement	1.0		
	- Prestressed concrete	0.10		
Indian Code IS 456: 2000	- Concrete containing metal and steam cured at elevated temperatures and prestressed concrete			0.4 ^a
	- RC or plain concrete containing embedded metal			0.6 ^a
	- Concrete not containing embedded metal or any material requiring protection from chlorides			3.0 ^a
Cement Association of Canada	- RC exposed to a moist environment or chlorides or both	0.15		
	- RC was exposed to neither a moist environment nor chlorides	1.00		
	- Prestressed concrete	0.06		

^a Expressed as kg/m³

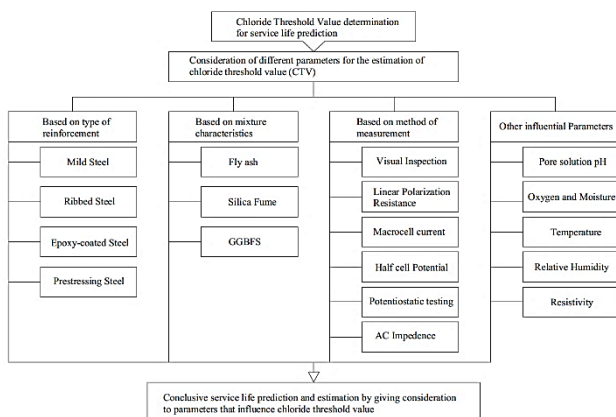


Fig. 1. Flowchart for the variables that impact the threshold value for chloride [19].

In previous studies, most researchers used de-ionized water or distilled water in the preparation of synthetic concrete pore solution (SCPs), which may not reflect the

composition of pore solution in the concrete. So, this work aims to study the corrosion behavior of high tensile strength of carbon steel in SCPs prepared with tap water, to obtain a more accurate C_{crit} value, with and without sodium chloride. In addition, anodic polarization and visual inspection were used in specifying the C_{crit} value and compared it with previous research values. Furthermore, Tafel polarization was used to determine the corrosion rate.

2. Experimental work

2.1. Sample preparation

High tensile strength of carbon steel rebar grades 80 with a minimum yield strength of (550 MPa), as specified in ASTM A615 standard specification [20]. Before preparing samples for electrochemical measurements, the reinforcing steel was tested for physical and chemical tests. The nominal diameter of the rebar steel was (16mm) and the physical test results are indicated in Tab. 2 and Fig. 2. The chemical composition test, including elemental analysis, using Spark Atomic Emission

Spectrometry and was conducted according to ASTM E415 [21]. The test results are indicated in Tab. 3.

Table 2. Physical tests, according to ASTM A615-15, for Grade 80 [550 MPa].

Bar Designation No. 16	Test results	Minimum Requirements
Tensile strength, (MPa)	732	690
Yield strength, (MPa)	602	550
Elongation in [200 mm], (%)	9.5	7
Nominal mass, (kg/m)	1.578	
94 % of the nominal mass, (kg/m)	1.553	1.483
Bend Test ^A , Pin Diameter = 5d ^B	No crack	No crack

^A Test bends 180°

^B d = nominal diameter of specimen

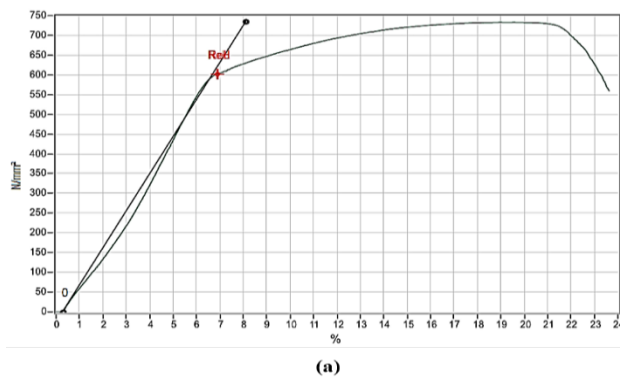


Fig. 2. Physical tests of rebar steel, a- Tensile testing curve, b- Bending test.

Table 3. Chemical composition of carbon steel rebar, grade 80 (expressed as weight percent).

Elements	%Wt.
Fe	98,3
C	0,145
P	0,022
S	0,035
Si	0,130
Mn	0,847
Cr	0,0595
Mo	< 0,0040
Ni	0,128
Al	0,0116

Co	0,0834
Cu	0,0557
Nb	0,0085
Ti	0,0110
V	0,0097
W	0,176
Pb	0,0158
Zr	0,0030

The microstructure of the rebar steel was performed on the cross-sectional area of a small sample of the steel. The sample was mounted with cold epoxy resin, and the surface was grounded, polished to mirror-like, and then etched with a 2% Nital solution. The microstructure was shown in the Fig. 3.

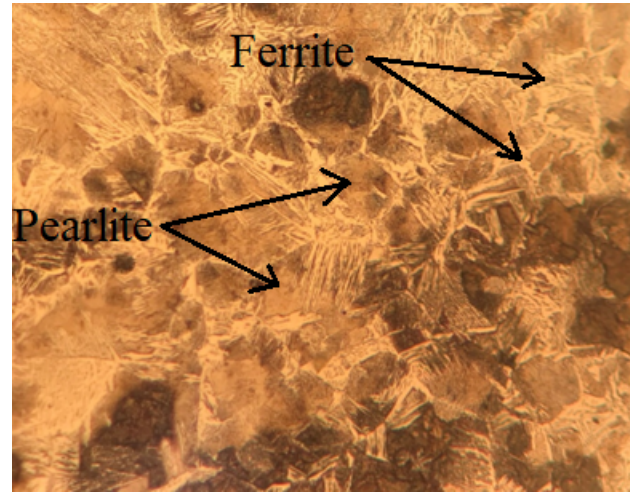


Fig. 3. Micro-structure of rebar grade 80, Magnification 500X.

After the test samples met the requirements of ASTM A615, then samples for the electrochemical test were prepared. In order to study the corrosion, the samples were cut, machined, and tapped into cylindrical samples of (9.5 ±0.1mm) in diameter and (12.7 ±0.1mm) in height with an exposed surface area of about (5 cm²), excluding the contact surface area between the sample and sample holder. Then all samples were wet ground with 240 grit silicon carbide paper and then wet polished with 600 grit silicon carbide paper to remove the coarse scratches. The samples were then cleaned with acetone and de-ionized water before being air dried, according to the standard test method ASTM G5-14 [22].

2.2. Test Solution preparation

Across many researches, simulating concrete pore solutions (SCPs) with the chemical compositions presented in Tab. 4 were used to evaluate the electrochemical behavior of rebar steel [23-26]. However, in this study the same electrolyte chemical composition was used except tap water was used rather than de-ionized or distilled water to simulate the concrete environment. The chemical composition of the tap water was indicated in Tab. 5, and it is conforming to the requirements of standard specification ASTM C1602 [27].

Furthermore, sodium chloride (NaCl) was added to the (SCPs) in concentrations, as weight percent, of (0.5, 1.0, 1.5, and 2.0% wt.). Consequently, four groups of solutions were used in this investigation. All reagents used in this study are of analytical grade purity. The solutions are prepared by using a magnetic stirrer for two hours to ensure the complete dissolution of the chemical reagents. The volume of each test solution in the corrosion cell was one liter. The benefit of doing the tests in the solution instead of the concrete has been

that the steel bars' surface can be visually inspected throughout the testing period, and the findings may be achieved quickly. The use of solution rather than real concrete also eliminates concrete resistance, which was one of the causes that limited the current flow. The general properties of these solutions at room temperature (25±1 °C) are listed in Tab. 6.

Table 4. Chemical compositions and pH of the simulated concrete pore solution.

Chemical agents	Concentration
NaOH, Mol/L	0.1
KOH, Mol/L	0.3
Ca(OH) ₂ , Mol/L	0.03
CaSO ₄ .H ₂ O (gypsum), Mol/L	0.002
pH	12.9

Table 5. Chemical composition of the tap water.

Parameters	Test results
pH	7.11
EC, μS/cm	787
TDS, mg/l	491.5
DO, mg/l	8.1
CO ₃ , mg/l	16
HCO ₃ , mg/l	104
Total Alkaniti, mg/l	120
Ca, mg/l	72
Mg, mg/l	54.65
Cl, mg/l	63.7
NO ₃ , mg/l	2.624
SO ₄ , mg/l	171.36
Na, mg/l	37.82
K, mg/l	4.1

Table 6. General properties of simulating concrete pore solutions with different chloride concentrations prepared with tap water.

Parameters	Sodium chloride concentration, %wt.				
	0	0.5	1.0	1.5	2.0
pH	12.95	12.86	12.77	12.68	12.51
Electrical conductivity, mS/cm	90.7	93.0	95.3	97.7	103.3
Salts, %	5.7	5.8	6.0	6.2	6.7
Specific gravity	1.042	1.044	1.045	1.046	1.049

2.3. Electrochemical measurements

The tests were performed at room temperature using electrochemical computer-controlled potentiostats (Gamry series G 300). The measurements were taken using a standard corrosion cell with a three-electrode configuration, as shown in Fig. 4. The specimens prepared from the rebars and a larger surface area of two graphite rods functioned as the working and counter electrodes, respectively. As a reference electrode, a saturated calomel electrode (E = + 0.242 V compared to a typical hydrogen electrode) was used. Open-circuit potential, Tafel extrapolation, and cyclic polarization experiments were performed sequentially after the initial ten hours of stability of the specimen's potentials in the test electrolyte. All the electrochemical measurements were performed by using a Faraday cage and individual grounding for corrosion cell, to avoid electromagnetic fields that produce noise or current

fluctuations in the polarization curve. These noises may confuse with metastable pitting [28].

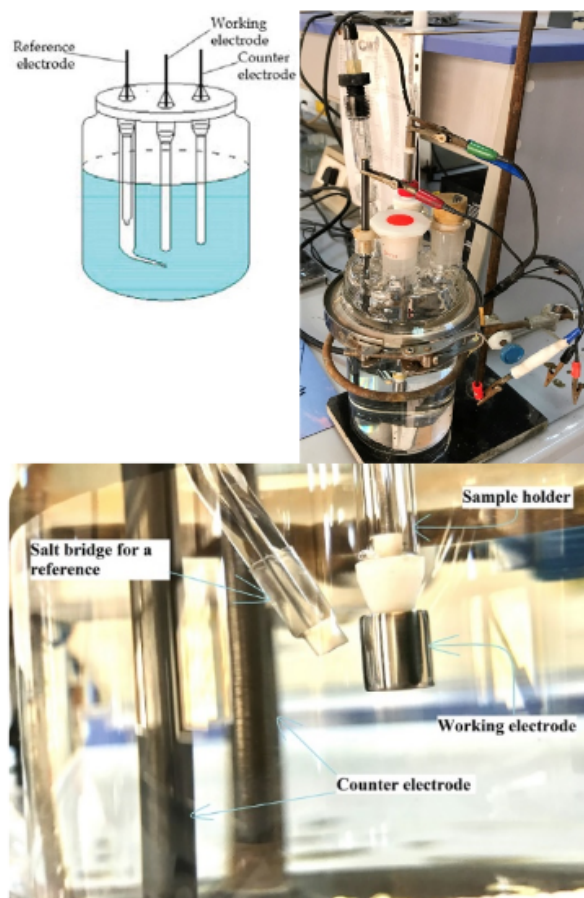


Fig. 4. Three-electrode configuration of the corrosion cell.

In order to conduct the Tafel test, the samples were polarized in the (-0.25 to +0.25) V/SCE range, with respect to the open circuit potential (OCP), with a scanning rate of 0.125 mV/s. The potential (E_{corr}) and corrosion current densities (i_{corr}) of the specimens were obtained using the Tafel extrapolation technique. Gamry Echem software package was used to analyze the obtained results [29], in which Marquardt algorithm has been used in determining anodic slope (β_a), cathodic slope (β_c), I_{corr}, E_{corr}. In addition, the software use Eq. 1 in determining the corrosion rate (CR) [30]:

$$CR = i_{corr} \cdot K \cdot \frac{EW}{\rho} \tag{1}$$

Where: CR = corrosion rate (mm/year), i_{corr} = corrosion current density (A/cm²), K = constant (0.00327), EW = iron equivalent weight (27.92) [30], ρ = steel density (7.86 g/cm³) [20].

Potentiodynamic cyclic polarization was done in the forward scanning range of (-0.1V to +1.6V SCE relative to OCP) and reverse scanning range of (+1.6 to 0V relative to OCP) with forward and reverse potential sweep rate of 0.6V/h. However, the scanning direction was reversed (toward more active potentials) either when the potential reached (+1.6V), or when the current reached 5 mA (5 × 10³ μA), as specified by ASTM G61-86 (2014) [31]. This test method's objective is to determine a material's susceptibility to the start of localized corrosion, which occurs when the passive layer is ruptured and the anodic current grows rapidly.

Also, the surface was inspected by an optical microscope after each cyclic polarization test.

3. Results and Discussion

3.1. Open circuit potential (OCP)

Before starting any electrochemical test, the samples were immersed in the test solution for about ten hours, to stabilize the potential, then the (OCP) was measured for (300 sec.) as indicated in Fig. 5. Within the test period, stable potentials were attained throughout each solution, demonstrating the creation of a stable passive film in each solution. In addition, with increasing the chloride concentration, the (OCP) shifted to the noble direction at maximum for a solution containing (1% wt.) chloride and then shifted in the active direction.

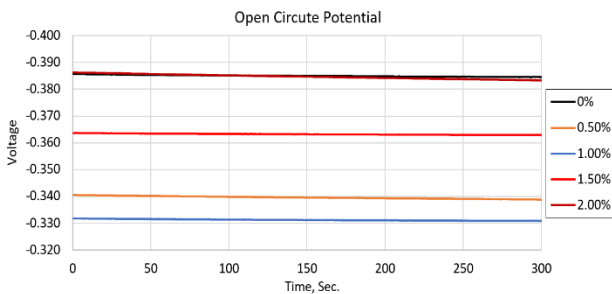


Fig. 5. OCP measurement with immersion time after ten hours of immersion.

This behavior may be attributed to the quality of oxide protective film that formed on the steel surface and/or the electrical conductivity of this passive film due to the complex nature of the test solution (SCPs, NaCl, and tap water). However, it is understandable to infer that all the rebar specimens developed in the various synthesized pore solutions will be in a passive status, as shown by the iron Pourbaix diagram, Fig. 6, given the pH range seen in concrete and our investigation.

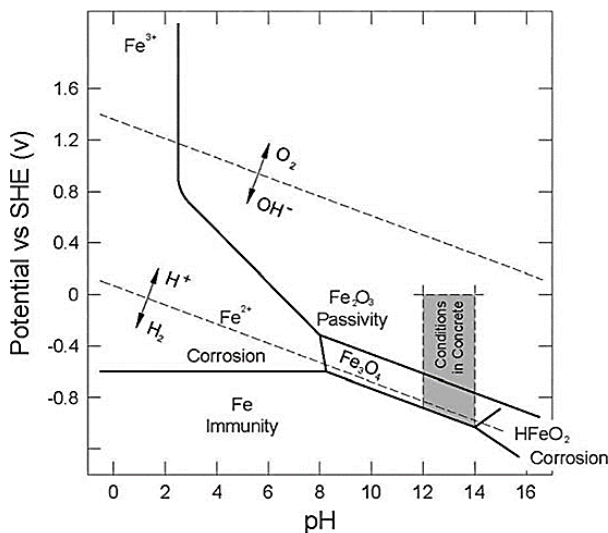


Fig. 6. Potential-pH (Pourbaix) diagram for iron-water at 25°C.

3.2. Tafel Polarization

Tafel curves were measured on the steel samples immersed in synthetic concrete pore solution with and without sodium chloride at different concentrations, as shown in Fig 7. All of the observed curves can be shown to have the same property,

which is an activation control present in both the anodic and cathodic branches. By using the Echem analytical program, the electrochemical parameters (Anodic slope, Cathodic slope, i_{corr} , E_{corr} , and Corrosion rate) were determined for all solutions and listed in table 7. The findings demonstrated that the cathodic branch slopes (β_c) are consistently less than the anodic branch slopes (β_a). This finding suggests that the anodic process is more controlled and that the anodic half-reaction has a greater impact on the i_{corr} than the cathodic reaction. The corrosion potential, current, and rate related to chloride concentration are more illustrated in Fig. 8.

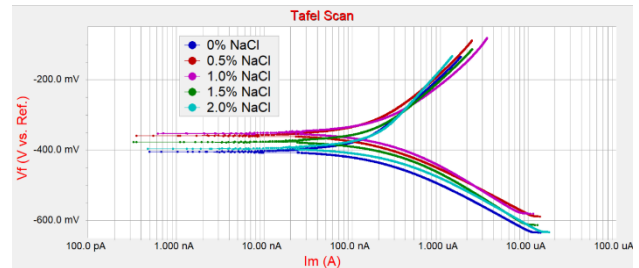


Fig. 7. Tafel tests for rebar specimen immersed in SCPs containing different chloride concentrations.

Table 7. Electrochemical parameters for rebar steel (grade 80) at different solutions.

Test parameters	NaCl addition, weight percent				
	0	0.5	1.0	1.5	2.0
Beta A, V/decade	0.248	0.222	0.200	0.244	0.305
Beta C, V/decade	0.112	0.121	0.136	0.125	0.112
i_{corr} , nA	143	167	214	197	188
E_{corr} , mV	-400	-357	-350	-373	-392
Corrosion Rate, $\mu\text{m}/\text{y}$	0.347	0.405	0.519	0.478	0.455

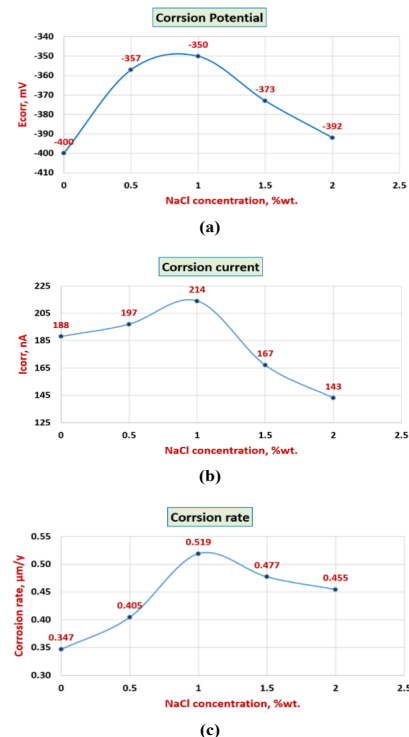
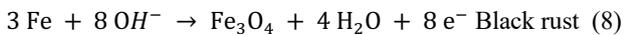
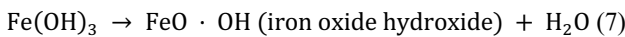
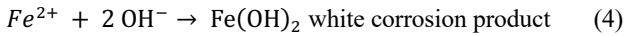
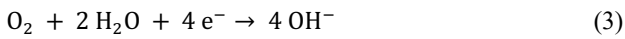
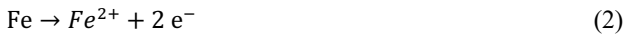
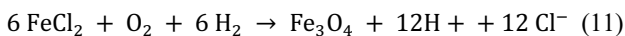
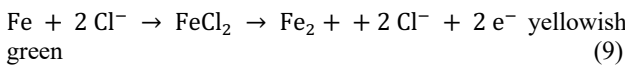


Fig. 8. Illustration graph for test parameters in relation to NaCl addition, a- corrosion potentials, b-corrosion currents, and c- corrosion rates.

The behavior of corrosion potential, fig. 10 (a), indicates the same behavior of OCP, in which there is a positive shift from (-400 mV, without chloride addition) to (-350 mV, with 1% wt. NaCl), and then followed by a negative shift to (-392 mV, with 2% wt. NaCl). However, the corrosion current and corrosion rate, figures 10-b and 10-c, were increased from (0.188 μ A) and (0.347 μ m/year) without chloride addition, to a maximum of (0.214 μ A) and (0.519 μ m/year) at the addition of (1% wt. NaCl), respectively. After that, 1% wt. NaCl, both corrosion current and corrosion rate were decreased gradually to (0.143 μ A) and (0.455 μ m/year) at the addition of (2% wt. NaCl), respectively. The reduced corrosion rates at increasing sodium chloride concentrations are explained by a gradual decrease in oxygen solubility in solution as sodium chloride concentration increases. The initial increment seems to be associated with an alteration of a diffusion-barrier oxide film's protective properties that develop on corroding iron (steel) surface. The corrosion reactions between rebar surface and concrete pore solution can be represented as follows [32]:



At high chloride concentrations:



According to hydroxide ions (OH) developing at cathodes, reaction (3), which are always near to Fe²⁺ ions formed by the anode and cause a film of Fe(OH)₂, reaction (4), to be present beside and adhering to a steel surface. Diffusion-barrier properties are provided by this film. However, because of the higher conductivity of sodium chloride solutions, more anodes and cathodes may work at considerably larger distances from one another. At these cathodes, NaOH, KOH, Ca(OH)₂, and CaSO₄.H₂O does not combine immediately with FeCl₂ generated by anodes; instead, these compounds dissolve into the solution and then react to produce Fe(OH)₂ apart from a metal surface. Any Fe(OH)₂ that is so generated does not act as a barrier layer to protect the metal's surface. Due to the increased ability of dissolved oxygen to reach cathodic regions, iron corrodes more quickly in diluted sodium chloride solutions. Consequently, beyond 1% NaCl, the continued drop in oxygen solubility takes precedence over any changes to the diffusion-barrier layer, which results in a reduction in corrosion rate [33].

3.3. Cyclic polarization

As illustrated in Fig. 9, cyclic potentiodynamic curves were obtained for reinforcing steel samples that were submerged in a synthetic concrete pore solution contaminated with sodium chloride at various concentrations. A clearly-defined passive zone is where the current seemed to be unaltered, and the Tafel region is where it relatively increased. During the potential rising, the sample loses its de-passivation and achieves its passive potential (E_{pa}) or passive current (I_{pa}). The curve without a distinct inflection point, passive potential or current for this case is assumed to be the tangent of the curve between the Tafel area and the passive region. Similarity for inflection point of pitting potential (E_p). consequently, all the important electrochemical parameters were obtained and listed in Tab. 8.

Table 8. Test results from cyclic polarization cures.

Test parameters	NaCl addition, weight percent			
	0%	0.5%	1.0%	1.5%
Pitting potential (E _p), mV	555.2	565.8	550.1	382.3
Protection potential (E _{prot}), mV	537.6	537.1	533.8	-
Protection current (I _{pro}), μ A	10.67	12.23	6.95	-
E _{corr(R)} , mV	25.67	11.93	-23.27	-
Passive potential (E _{pa}), mV	123.6	125.3	120.3	121.4
Passive current (I _{pa}), μ A	6.53	7.57	5.40	0.848

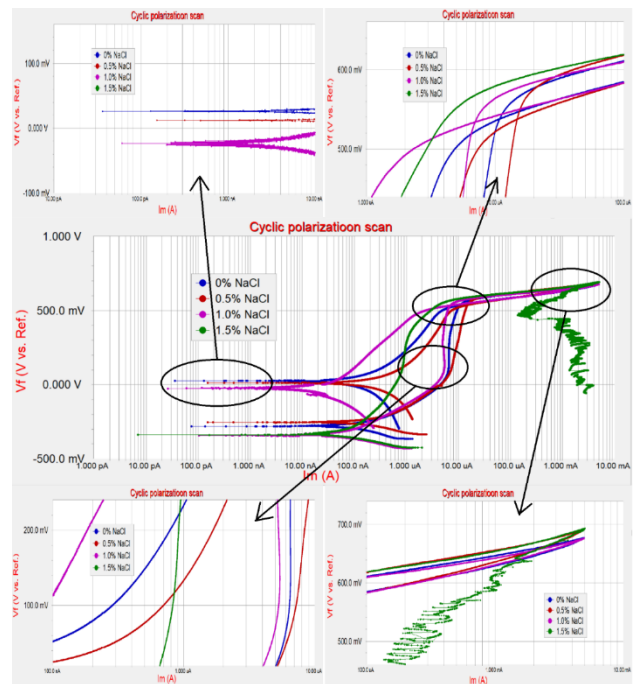


Fig. 9. Potentiodynamic cyclic polarization curves for rebar samples with different percentages of NaCl addition.

Obviously from Fig. 9 and Tab. 8, all the curves had approximately the same values of the passive potential of (~120 mV) for all solutions, but the passive currents (I_{pa}) are different and can be illustrated in Fig. 10. It seems to be the values of pH, conductivity, and chloride in the solutions presented in Tab. 6 have no significant influence on the

passive current densities (I_{pa}). These results suggest that the cyclic polarization curves may have more complex predictor variables and/or the oxide films that develop on the rebar surface may be the source of the observed differences and that the synthetic pore solution used to grow the oxide layer has an impact on the oxide layer quality, as relatively low passive current density indicates higher quality and vice versa. Also, metal loss rates will increase as a result of greater passive current densities, making these oxides less protective and consequently of lower quality. This hypothesis is true when there are no chloride ions in the solution, but in case of its presence with other ions in the test solution during immersing time, they accelerate the iron dissolution (Fe^{2+}), reaction (4) and (9), from the surface and between metal substrate and oxide barrier of the passive film [34]. So that, the quality and/or thickness of this passive film would be increased during the anodic polarization, and thus lower passive currents are indicated in polarization curves when chloride concentration increases. But, the ratio of dissolution/re-passivation rates at higher potentials ($> +600$ mV) is increased when chloride concentration increases until a critical concentration of (1% NaCl) then stable pits are formed beyond this concentration and the steel fails to re-passivated the surface at these conditions.

The oxygen evolution process caused the current to grow quickly when the voltage reached the maximum level (over +550 mV) [25, 35-37], except the curve of addition of 1.5% NaCl showed two inflection points. The first represents E_p , while the second inflection represents the oxygen evolution potential. So, the E_p cannot be specified in a natural aerated solution with less than 1.5% NaCl addition. The sudden rise in current caused by the development of one or even more stable pits on steel surface provide an indicator of the pitting potential (E_p). However, the hypothesis described above does not apply to the development of a stable pit; it only refers to passivity loss. Many congregations of various passivity breakdown sites, such as grain boundaries, oxide and carbide precipitates, MnS inclusions, etc., may be found on any metal surface and act as microchemical/microstructural discontinuity within the barrier layer of the passive film. As a result, a structural discontinuity develops where a precipitate meets a barrier layer. This discontinuity provides a pathway between the barrier layer's exterior and a metal substrate that is expected to have a higher ions vacancy diffusivity [38]. However, all the curves showed passivity loss, but only the curve containing 1.5% NaCl developed stable pits, as indicated in Fig. 12-d.

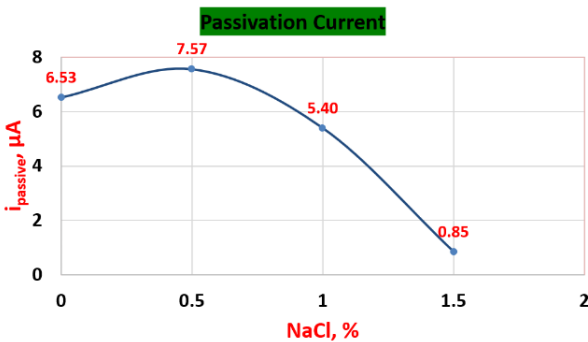


Fig. 10. Illustration graph for passivation currents at different NaCl addition.

Generally, metal corrosion often goes through two processes, from passivation to pitting. Metastable pitting is the first, and de-passivation or the formation of steady-state

pitting is the second. Most often, metastable pitting will evolve into steady state pitting. Before the pitting of metallic and alloyed materials, tiny current fluctuations are noticed, which are the consequence of metastable pits on the surface being nucleated, grown, and re-passivated [28, 39, 40]. These very small current fluctuations can be observed in solutions containing 1% NaCl, and it is clearly noticed in the reversed potential at regions near to reversed corrosion potential ($E_{corr(R)}$), Fig. 12-b, confirming the formation of metastable pits on the rebar surface.

During the reversed polarization plots, a new corrosion potential ($E_{corr(R)}$) that is the result of the creation of an additional set of anodic/cathodic curves is shown in Fig. 9. In comparison to the forward corrosion potentials for each solution, the new corrosion potentials created during the reverse-scanning are nobler. Furthermore, these potentials are shifted to the active direction when the chloride concentrations are increased, as indicated in Fig. 11. These corrosion potentials can be explained by the formation of a new phase in the passive film created by the forward polarization of the rebar surface. Iron cations seem to have moved through the pore spaces of the oxide layer as a result of the anodic dissolution of the ferrite and pearlite microstructures. These ions reacted with water and dissolved oxygen in the solution to produce iron oxides of the thicker and more protective layer due to higher potential. These findings show that it is possible to develop appropriate ways to enhance the protective layer that covers reinforcing bars' surfaces before inserting them into concrete [41].

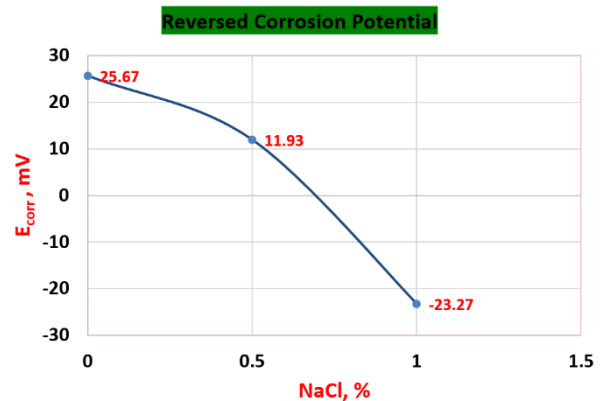


Fig. 11. Illustration graph for reversed corrosion potentials ($E_{corr(R)}$) with NaCl addition.

3.4. Surface morphologies

3.4.1. Optical microscope

The visual inspection of the surface morphology for rebar specimens after anodic polarization in a sodium chloride-containing SCPs is seen in Fig. 12 with magnification of (500X). As indicated in Fig. 12-a, the addition of 5% NaCl doesn't show any initiation of pitting corrosion. Whereas the addition of 1% NaCl to the SCPs, Fig. 12-b, showed that the surface contains a very large number of microscope sizes of passivated metastable pitting. However, with the addition of 1.5%, Fig. 12-c, indicated the surface loses the passivation layer and stable pits are formed.

3.4.2. SEM-EDX

The SEM morphologies of the reinforcing steel after anodic polarization in SCPs contaminated with 1.5 percent NaCl are shown in Fig. 13. The image indicates the randomly arranged, many flowers-like formations that were produced on the steel

rebar surface. These hierarchical structures that resemble flowers match the morphologies of goethite (α -FeOOH) or α -Fe₂O₃/ γ -Fe₂O₃, which shows that significant corrosion has taken place on the rebar surface. Additionally, it has been shown that laminar structures, which match the morphologies of the iron hydroxide/ γ -FeOOH (lepidocrocite) [42, 43].

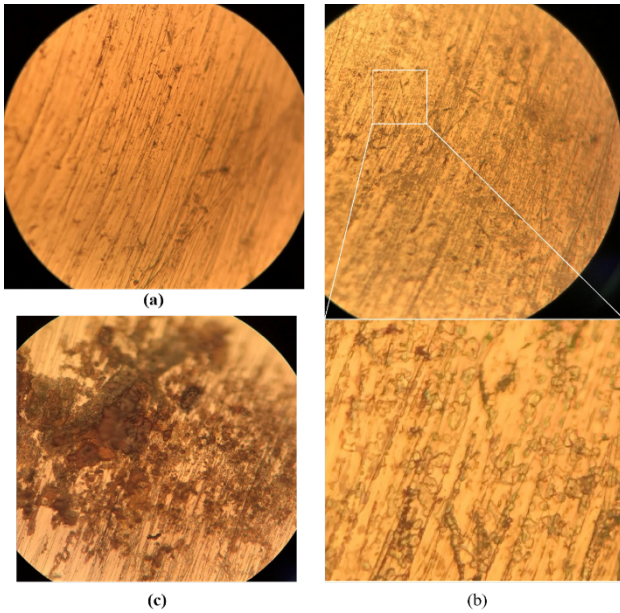


Fig. 12. Optical image for rebar surface after cyclic polarization tests with 500X magnification. (a) 0.5% NaCl addition, (b) 1.0% NaCl addition, (c) 1.5% NaCl addition.

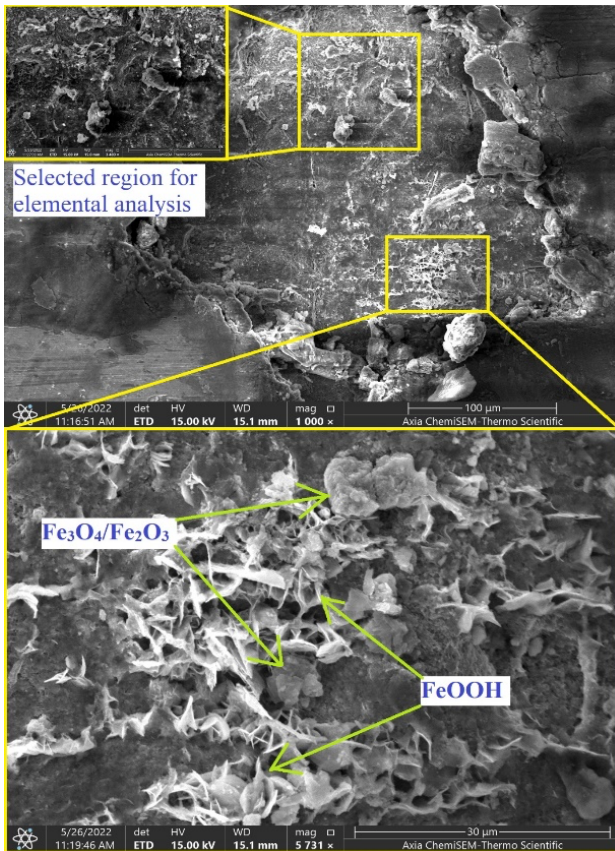


Fig. 13. SEM images for the corroded surface of rebar sample after cyclic polarization with 1.5% NaCl addition.

The chosen location in the illustration Fig. 13 was likewise subjected to an EDS analysis. On the steel rebar surface, it was found that the three main elements were iron, oxygen, and chlorine, as indicated in Fig. 14 and Tab. 9. Additionally, sulfur and manganese were found, which may have been driven mostly by MnS inclusions that are the most common cause of pitting corrosion initiation in chloride-contaminated SCPs. The production of iron oxide on the steel surface was confirmed by the elemental composition.

Table 9. EDS analysis for corrosion products.

Element	Atomic %	Atomic % Error	Weight %	Weight % Error
C	14.6	0.2	5.6	0.1
O	40.5	0.4	20.8	0.2
Na	4.1	0.1	3.0	0.1
S	0.3	0.0	0.3	0.0
Cl	1.4	0.1	1.6	0.1
K	2.8	0.1	3.5	0.1
Cr	0.4	0.0	0.6	0.1
Mn	1.1	0.1	1.9	0.3
Fe	35.0	0.3	62.8	0.6

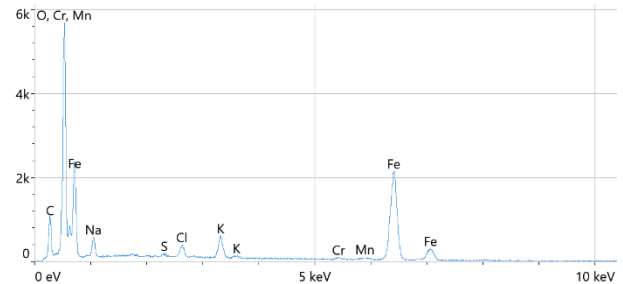


Fig. 14. EDS analysis graph for selected region on the steel surface.

4. Conclusions

The use of the Tafel polarization approach for determining the corrosion rate for passive metals or alloys in SCPs may not be very accurate for tested conditions, natural aerated solution and tap water, because the oxide layer that formed close to the rebar surface act as a barrier layer that limits the current transfer between the working and counter electrodes.

The cyclic polarization test yielded important knowledge on the active, passive, and trans-passive regions; and the pitting nucleation process in various chloride environments. However, the findings of the experiment show that the E_p and E_{prot} cannot be specified in a natural aerated solution, due to oxygen evolution at potentials of about 550mV. The chloride thresholds for carbon steel determined using the potentiodynamic cyclic polarization approach were in compliance with relevant literature. The progressive chloride addition experiments produced a chloride critical level of 0.5% NaCl is appropriate for these environments. Because metastable pits developed on the steel surface after the addition of 1 % NaCl, these pits may have become active and propagate over time as temperatures rise, reducing the pH of the concrete pore solution due to carbonation or leaching, stray current, etc.

This is an Open Access article distributed under the terms of the Creative Commons Attribution License.



References

- James, A., Bazarchi, E., Chiniforush, A. A., Aghdam, P. P., Hosseini, M. R., Akbarnezhad, A., Martek, I. & Ghodoosi, F. "Rebar corrosion detection, protection, and rehabilitation of reinforced concrete structures in coastal environments: A review". *Construction and Building Materials*, 224, 2019, pp. 1026-1039.
- Marcos-Meson, V., Michel, A., Solgaard, A., Fischer, G., Edvardsen, C. & Skovhus, T. L. "Corrosion resistance of steel fibre reinforced concrete-A literature review". *Cement and Concrete Research*, 103, 2018, pp. 1-20.
- Kakooei, S., Akil, H. M., Dolati, A. & Rouhi, J. "The corrosion investigation of rebar embedded in the fibers reinforced concrete". *Construction and Building Materials*, 35, 2012, pp. 564-570.
- Liu, Y., Song, Z., Wang, W., Jiang, L., Zhang, Y., Guo, M., Song, F. & Xu, N. "Effect of ginger extract as green inhibitor on chloride-induced corrosion of carbon steel in simulated concrete pore solutions". *Journal of cleaner production*, 214, 2019, pp. 298-307.
- Goni, S. & Andrade, C. "Synthetic concrete pore solution chemistry and rebar corrosion rate in the presence of chlorides". *Cement and Concrete Research*, 20(4), 1990, pp. 525-539.
- Akbari, A., Nikookar, M. & Feizbahr, M. "Reviewing Performance of Piled Raft and Pile Group Foundations under the Earthquake Loads". *Research in Civil and Environmental Engineering*, 1(5), 2013, pp. 287-299.
- Kakooei, S., Akil, H. M., Jamshidi, M. & Rouhi, J. "The effects of polypropylene fibers on the properties of reinforced concrete structures". *Construction and Building Materials*, 27(1), 2012, pp. 73-77.
- Malik, A. U., Ahmad, S., Andijani, I. & Al-Fouzan, S. "Corrosion behavior of steels in Gulf seawater environment". *Desalination*, 123(2-3), 1999, pp. 205-213.
- Shreir, L., "Corrosion: Vol. 2, Corrosion Control". Georges Newnes Limited. 1963.
- Betts, A. & Boulton, L. "Crevice corrosion: review of mechanisms, modelling, and mitigation". *British corrosion journal*, 28(4), 1993, pp. 279-296.
- McCafferty, E., *Crevice corrosion and pitting*, in *Introduction to Corrosion Science*: Springer. 2010, pp. 263-313.
- Obeyesekere, N. U. "Pitting corrosion". *Trends in Oil and Gas Corrosion Research and Technologies*, 2017, pp. 215-248.
- Angst, U., Elsener, B., Larsen, C. K. & Vennesland, Ø. "Chloride induced reinforcement corrosion: rate limiting step of early pitting corrosion". *Electrochimica Acta*, 56(17), 2011, pp. 5877-5889.
- Chalhoub, C., François, R. & Carcasses, M. "Determination of chloride threshold initiating corrosion: A new set-up taking the localized aspect of corrosion into account". *Cement and Concrete Research*, 124, 2019, pp. 105825.
- Glass, G., Page, C. & Short, N. "Factors affecting the corrosion rate of steel in carbonated mortars". *Corrosion Science*, 32(12), 1991, pp. 1283-1294.
- Chalhoub, C., François, R. & Carcasses, M. "Critical chloride threshold values as a function of cement type and steel surface condition". *Cement and Concrete Research*, 134, 2020, pp. 106086.
- Angst, U., Elsener, B., Larsen, C. K. & Vennesland, Ø. "Critical chloride content in reinforced concrete—A review". *Cement and concrete research*, 39(12), 2009, pp. 1122-1138.
- Yousri, K. M., Osman, T. A. & El-Shimy, E. "International Standards and codes For Chloride Limits in Reinforced Concrete Structures".
- Mahima, S., Moorthi, P., Bahurudeen, A. & Gopinath, A. "Influence of chloride threshold value in service life prediction of reinforced concrete structures". *Sādhanā*, 43(7), 2018, pp. 1-19.
- ASTM A615/A615M-15a, *Standard Specification for Deformed and Plain Carbon-Steel Bars for Concrete Reinforcement*, in *ASTM International: West Conshohocken, PA, USA*. 2015.
- ASTM E415 – 17, *Standard Test Method for Analysis of Carbon and Low-Alloy Steel by Spark Atomic Emission Spectrometry*, in *ASTM International: West Conshohocken, PA, USA*. 2017.
- ASTM G5-14, *Standard Reference Test Method for Making Potentiodynamic Anodic Polarization Measurements*, in *ASTM International: West Conshohocken, PA, USA*. 2014.
- Figueira, R. B., Sadoyski, A., Melo, A. P. & Pereira, E. V. "Chloride threshold value to initiate reinforcement corrosion in simulated concrete pore solutions: The influence of surface finishing and pH". *Construction and Building Materials*, 141, 2017, pp. 183-200.
- Dong, Z. & Poursaeae, A. "Corrosion behavior of coupled active and passive reinforcing steels in simulated concrete pore solution". *Construction and Building Materials*, 240, 2020, pp. 117955.
- Behera, P. K., Misra, S. & Mondal, K. "Corrosion behavior of strained rebar in simulated concrete pore solution". *Journal of Materials Engineering and Performance*, 29(3), 2020, pp. 1939-1954.
- Torbati-Sarraf, H. & Poursaeae, A. "Study of the passivation of carbon steel in simulated concrete pore solution using scanning electrochemical microscope (SECM)". *Materialia*, 2, 2018, pp. 19-22.
- ASTM C1602/C1602M-12, *Standard Specification for Mixing Water Used in the Production of Hydraulic Cement Concrete*, in *ASTM International: West Conshohocken, PA, USA*. 2012.
- Tang, Y., Zuo, Y., Wang, J., Zhao, X., Niu, B. & Lin, B. "The metastable pitting potential and its relation to the pitting potential for four materials in chloride solutions". *Corrosion Science*, 80, 2014, pp. 111-119.
- Gamry instruments. "An Overview of Gamry Software". Retrieved from: <https://www.gamry.com/support-2/software/>, 2010-03-11/2022-07-13.
- ASTM G102-89, *Standard practice for calculation of corrosion rates and related information from electrochemical measurements*, in *ASTM International: West Conshohocken, PA, USA*. 2010.
- ASTM G61-86 (2014), *Standard Test Method for Conducting Cyclic Potentiodynamic Polarization Measurements for Localized Corrosion Susceptibility of Iron-, Nickel-, or Cobalt-Based Alloys I*, in *ASTM International: West Conshohocken, PA, USA*. 2014.
- Thangavel, K., *The threshold limit for chloride corrosion of reinforced concrete*. 2004, De Gruyter.
- Revie, R. W., "Corrosion and corrosion control: an introduction to corrosion science and engineering". John Wiley & Sons. 2008.
- Hussain, R. R. "Passive layer development and corrosion of steel in concrete at the nano-scale". *Journal of Civil & Environmental Engineering*, 4(3), 2014, pp. 1.
- Moreno, M., Morris, W., Alvarez, M. & Duffó, G. "Corrosion of reinforcing steel in simulated concrete pore solutions: Effect of carbonation and chloride content". *Corrosion Science*, 46(11), 2004, pp. 2681-2699.
- Moser, R. D., Singh, P. M., Kahn, L. F. & Kurtis, K. E. "Chloride-induced corrosion resistance of high-strength stainless steels in simulated alkaline and carbonated concrete pore solutions". *Corrosion Science*, 57, 2012, pp. 241-253.
- Addari, D., Elsener, B. & Rossi, A. "Electrochemistry and surface chemistry of stainless steels in alkaline media simulating concrete pore solutions". *Electrochimica Acta*, 53(27), 2008, pp. 8078-8086.
- Macdonald, D. D., Qiu, J., Sharifi-Asl, S., Yang, J., Engelhardt, G. R., Xu, Y., Ghanbari, E., Xu, A., Saatchi, A. & Kovalov, D. "Pitting of carbon steel in the synthetic concrete pore solution". *Materials and Corrosion*, 72(1-2), 2021, pp. 166-193.
- Pistorius, P. & Burstein, G. "Growth of corrosion pits on stainless steel in chloride solution containing dilute sulphate". *Corrosion science*, 33(12), 1992, pp. 1885-1897.
- Laycock, N. & Newman, R. "Localised dissolution kinetics, salt films and pitting potentials". *Corrosion science*, 39(10-11), 1997, pp. 1771-1790.
- Hussain, R., Singh, J., Alhozaimy, A., Al-Negheimish, A., Bhattacharya, C., Pathania, R. & Singh, D. "Effect of Reinforcing Bar Microstructure on Passive Film Exposed to Simulated Concrete Pore Solution". *Aci materials journal*, 115(2), 2018.
- Thalib, S., Ikhsan, M., Fonna, S., Huzni, S. & Ridha, S. "Identification of corrosion product on medium carbon steel under the exposure of Banda Aceh's atmosphere". In *IOP Conference Series: Materials Science and Engineering*, IOP Publishing: 2018, pp. 012004.
- Raghav, M., Karthick, S., Park, T. & Lee, H.-S. "Assessment of corrosion performance of steel rebar in snail shell ash blended cements under marine environments". *Materials*, 14(23), 2021, pp. 7286.